Cellular automata simulations on nanocrystallization processes: From instantaneous growth approximation to limited growth

J.S. Blázquez, C.F. Conde, A. Conde,

Departamento de Física de la Materia Condensada, ICMSE-CSIC, Universidad de Sevilla, P.O. Box 1065, 41080, Sevilla, Spain

Abstract

Cellular automata simulations have been performed to simulate the crystallization process under a limited growth approximation. This approximation resembles several characteristics exhibited by nanocrystalline microstructures and nanocrystallization kinetics. Avrami exponent decreases from a value n = 4 indicating interface controlled growth and constant nucleation rate to a value n ~ 1 indicating absence of growth. A continuous change of the growth contribution to the Avrami exponent from zero to 3 is observed as the composition of the amorphous phase becomes richer in the element present in the crystalline phase.

Research Highlights

► Low values of the Avrami exponent can be explained in terms of an instantaneous growth process or a limited growth process. ► Microstructure and kinetics predicted by celular automata under this approximation reproduces the experimental results. ► Compositional and growth range effects are explored.

Keywords

Nanocrystallization kinetics; Cellular automata; Avrami exponent

1. Introduction

Nanocrystalline alloys obtained from controlled devitrification as primary crystallization products of precursor amorphous alloys are characterized by the presence of tiny crystallites (5–20 nm) embedded in a residual amorphous matrix with different composition. The kinetics of nanocrystallization process is atypical, because the density of nuclei is extraordinarily high in comparison with that of conventional microstructures obtained from devitrification [1] and [2].

Scientific community is paying attention to these systems not only from a fundamental point of view but also due to a wide range of physical properties [3], [4] and [5] which are enhanced in nanocrystalline systems with respect to conventional microstructures with micrometric crystals, making nanocrystalline alloys very interesting systems for technological applications.

Growth impingement has been considered as the responsible for the very low growth kinetics, enabling a very significant nucleation in extended time (isothermal) or thermal (non-isothermal) regimes. Recently, an instantaneousg rowth approximation was proposed assuming that each formed nucleus grows to its saturation value instantaneously and afterwards no longer growth is allowed. The instantaneous growth approximation[6] enables a successful and simple explanation of the nanocrystallization kinetics on the frame of Jhonson–Mehl–Avrami–Kolmogorov (JMAK) theory, ascribing the very low Avrami exponent, ~ 1, to the fact that only nucleation mechanisms affect the global kinetics. In fact, it is experimentally observed that crystal growth is so quickly impinged that the time required for a nucleus to grow up to its saturation size is negligible compared to the time required for the complete transformation process of nanocrystallization.

Computer simulations have successfully described crystallization kinetics using different methods: Montecarlo [7] and [8], molecular dynamics [9] or celular automata[10], [11] and [12]. In particular, celular automata simulations could reproduce the kinetics and microstructure observed in Cu free and Cu containing Hitperm alloys [13], where the size of the crystalline units is about 5 nm. The assumption of two different nucleation mechanisms allowed us to understand the effect of Cu addition and the formation of agglomerates in Cu free alloys, as well as the microstructural dependence with Co content in the alloy.

In this work, the instantaneous growth approximation is extended to a limited growth approximation in a new set of cellular automata simulation experiments, allowing the crystallites to grow during a limited time (a certain number of iteration steps) before they become blocked. This extension of the instantaneous growth approximation will take into account those nanocrystalline systems where the crystal size is large enough to evidence crystal growth during the transformation.

The goal of the work will be to describe the well known experimental results on nanocrystalline systems: slow kinetics, low Avrami exponents and refined microstructure [1], using simulations under this simple approach. Results derived in this study should be applicable to any nanocrystalline system obtained from devitrification of a precursor amorphous material.

2. JMAK crystallization theory

The classical JMAK theory of crystallization was developed by Johnson and Mehl [14], Avrami [15] and Kolmogorov [16] to describe the evolution of the crystalline fraction as a function of the annealing time taking into account the geometrical impingement between growing crystals [1]. Although this theory was developed for polymorphic transformations during isothermal treatments, it has been extended to non-isothermal regimes [17], [18], [19], [20] and [21] and to transformations in which the parent and product phases have different compositions [1] and [5]. JMAK theory predicts that the transformed fraction, X, evolves with annealing time at a certain isothermal temperature T as:

$$X=1-\exp\{-[K(T)(t-t0)]n\}$$

where K(T) is a frequency factor for which a thermal Arhenius dependence is assumed, t is the time, t0 is the incubation time and n is the Avrami exponent. In the following simulations, t0 is fixed to zero.

The key parameter of the theory is the Avrami exponent, which can be related with the mechanisms of nucleation and growth[22] as:

$n=nI+d\cdot nG$

where nI refers to nucleation (nI < 1 for decreasing nucleation rate, nI = 1 for a constant nucleation rate and nI > 1 for increasing nucleation rate), d is the dimensionality of the growth process and nG refers to growth (nG = 1 for interface controlled growth and nG = 0.5 for diffusion controlled growth) [22].

A local value of the Avrami exponent [23], n(X), can also be obtained for the isothermal regimes from the slope of the double logarithmic representation, ln[− ln(1 − X)] vs. ln(t), known as the Avrami plot:

$$n(X) = \frac{d\ ln[-\ ln(1-X)]}{d\ ln(t)}$$

In the case of instantaneous growth approximation, JMAK theory is valid to describe the results obtained from simulations of polymorphic transformations and is approximately valid for non-polymorphic transformations, although the maximum nucleation rate is shifted with respect to n = 1 value [24].

3. Simulation program

The simulation program used is an extension of the previous one describing the instantaneous growth process and detailed elsewhere [13]. In order to simplify the nucleation mechanism, “in contact” nucleation (preferential sites for nucleation) leading to the formation of agglomerates has been suppressed.

The celular automata simulation program considers a three (two) dimensional space divided in cubic (square) cells and the time is discretized in iteration steps. At the initial state, the system is homogeneously amorphous with a general composition Fe100−yExcy, being Fe the element forming the crystals and Exc the element which is expelled out of the crystals. The use of Fe to name the atom forming the crystalline phase does not reduce generality to the obtained results, which can be easily extended to Fe free nanocrystalline systems. Therefore, every cell is suitable to nucleate but in order to do so it must fulfil not only deterministic requisites (to be amorphous or to have enough Fe in the neighbourhood) but also the stochastic character of nucleation has to be taken into account. This is considered by randomly selecting a cell as candidate to develop a new crystalline nucleus and assigning a probability to nucleate depending on the Fe needed to complete the crystalline composition. If the Fe needed to crystallize is zero, the probability for nucleation of the chosen cell is 1.

After certain number of iteration steps, in which random nucleation is considered as described above, the whole space is explored to allow suitable crystallites to grow to their adjacent cells (if they are not already transformed). Crystals with a certain size are not allowed to grow further, following a limited growth approximation. The effective nucleation rate can be change varying the number of iteration steps of random nucleation between two growth steps. This value can be also tuned by changing the size of the explored space.

It is worth mentioning that the JMAK theory assumes a negligible size of the nuclei. Apparently this feature is not fulfilled in our simulations as the crystallites nucleate with a finite size (one cell) comparable to the final size, in some cases. However, the new nucleus in the simulation can be understood as a growing crystal which was formed an iteration step before with a null size. This explains why there is no effect of nucleus size on the kinetic parameters obtained in the simulations performed, although these effects have been reported by some authors [25].

4. Results

4.1. Polymorphic transformations

Although nanocrystalline systems are generally obtained during non polymorphic transformations, simulations concerning equicompositional amorphous and crystalline phases can help to clarify the effects of each parameter on the kinetics of transformation. Moreover, JMAK theory was developed to describe such transformations and thus is expected to be valid in the description of the simulations performed.

In these simulations, the probability for nucleation is 1 when there is no need of acquisition of Fe from outside the cell. Therefore, a new nucleus will be formed after each iteration step unless the chosen cell corresponds to an already transformed one (geometrical impingement), being the nucleation probability proportional to $(1 - X)$.

Fig. 1 shows the evolution of a selected 20 × 20 cell region in a 500 × 500 two dimensional simulated system during a polymorphic transformation. The initial time was chosen as that at which the first nucleus appears in the selected region. The differences between unlimited growth (Fig. 1a) and limitedgrowth (Fig. 1b) are evident. The initial nucleus grows for both systems as time increases and new nuclei can appear (moreover, other nuclei could be formed outside the region shown). For the system shown in Fig. 1b, the growth is limited to four iteration steps (GL = 4). In addition, at the edges of the region shown, some cells crystallize due to growth of crystals formed out of this region.

After comparison between limitedgrowth systems and those in which unlimited growth applies, the following consequences, typical for nanocrystalline systems, can be derived for limitedgrowth systems: slower kinetics, more homogeneous grain size distribution, crystals with a more regular shape and reduction of the number of grain boundaries.

Fig. 2 shows the evolution of the transformed fraction, X, as a function of iteration steps (time, t), as well as the Avrami plot and the local Avrami exponent obtained from the slope of the Avrami plot. Simulations were performed on a series of 500 × 500 cells, two dimensional systems, with different values of the growth limit.

For large growth limits, differences with unlimited growth processes are negligible: Before a crystal achieves its maximum size after GL steps, the geometrical impingement blocks the crystal growth. Large growth limits must be understood as relative to the size of the explored space. If GL exceeds the half of the linear size of the space, no crystal would stop growing before geometrical impingement occurs.

As the geometrical impingement is the only mechanism taken into account in JMAK theory, these systems are in agreement with JMAK theory predictions and a constant value of the local Avrami exponent is obtained, n = 3, for any value of crystalline fraction. This value can be explained as the sum of contributions from a constant nucleation (nI = 1, as the nucleation mechanism is constant along the simulation) and from an interface controlled growth in two dimensions (nG = 1).

Interface controlled growth is a consequence of the constant linear growth rate imposed to the simulations: after a constant number of iteration steps considering nucleation of randomly chosen cells, the adjacent cells of each crystal below its maximum allowed size are transformed. In the case of diffusion controlled growth, the linear growth rate should be proportional to the inverse of the square root of the time at the isotherm.

Nevertheless, analyses of the growth rate dependence on the crystal radius yielded an initial interface controlled growth followed by diffusion controlled growth for a primary phase growing in a supersaturated matrix [1]. This is a consequence of an initial transient due to non-steady conditions and to soft impingement [1]. Therefore, the step function of the growth rate considered for the simulations performed in the present study can be considered as an approximation to the actual growth rate (see Fig. 3 in ref. [1]).

As growth limit decreases, kinetics is slowed down and the Avrami exponent is no longer constant. Initially starts at n = 3, as for the unlimited growth case, but it decreases after achieving a certain value of crystalline fraction (larger as the limit growth increases).

Similar results are obtained in 3D systems, as shown in Fig. 3 for a 503 cells system. In this case, the constant value of the Avrami exponent for unlimited growth or very large limit growth processes is n = 4, in agreement with a three dimensional growth process.

4.2. Non-polymorphic transformations

If the compositions of the parent amorphous phase and of the product crystalline phase are different, the system cannot be properly described by JMAK theory. However, the theory is widely used after normalizing the transformed fraction to the maximum achievable value, Xmax. Experimentally, this value is obtained as the crystalline volume fraction of samples annealed up to the end of the nanocrystallization process (e.g. by X-ray diffraction). In the

simulations performed, Fe exhaustion would stop the transformation. However, only for very poor Fe containing alloys, Fe exhaustion in the amorphous matrix could be assumed as the factor stopping the nanocrystallization process [26], being Xmax close to the value obtained from a composition balance equation. In general, nanocrystallization process ends once the residual amorphous matrix is stabilized [1].

Assuming a complete exhaustion of Fe in the residual amorphous matrix, a theoretical maximum transformed fraction could be obtained for an initial amorphous composition Fe100−yExcy from a simple balance equation as:

$$X^{max} = \frac{100-y}{100}$$

However, the saturation values obtained during simulations are lower than the values obtained from Eq. (4). This can be explained by untransformed cells which were surrounded by low Fe containing cells or crystalline cells not allowed to grow further and, consequently, unable to transform. Therefore, the maximum transformed fraction used for normalization was the saturation value obtained in the simulations, in a similar way as it would be done for experimental data. Both values are linearly correlated as shown in Fig. 4.

In the simulations performed in this work, the Fe accessible to a cell is limited to that of a sphere with a diameter equal to the diagonal of the cell and distributed among its six neighboring cells. Therefore, if there is not enough Fe in the accessible surrounding, the crystal could grow only to some adjacent cells but not to all of them. This is because some next nearest neighbor cells are shared among cells candidates to crystallize but they cannot supply Fe to all of them so some of the candidates cannot be transformed. In order to clarify this point, Fig. 5 shows the number of cells of a single growing crystal without any geometrical impingement as a function of the Fe content. It can be observed that the crystal grows faster as the composition is richer in Fe content.

Although the effect is enhanced in the simulation performed due to the strong volume limitation for Fe acquisition, a qualitative behavior could be inferred from these data. For very low Fe content (< 37% Fe in our case) nucleation is not possible as there is not enough Fe in the allowed volume to enrich a single cell to 100% of Fe. For low Fe content, there is a compositional range (37–44% Fe) for which nucleation is possible but growth is totally banned. After the nucleus cell is enriched in Fe, the neighbor cells that should proceed to transform during the next iteration step become so exhausted in Fe that their surroundings (next nearest neighbor cells) cannot supply the Fe needed for them to reach 100% of Fe. In this case, the size of the crystal is limited to 1 cell. Other case occurs for crystals limited to 3 cells (45–46% Fe), as some neighbor cells are shared, if they contribute to the growth of one cell, they have not enough Fe to contribute to another one and the growth is stopped. This would be a case of self-limited growth. For higher Fe concentrations, the crystal continuously grows and faster as the system is richer in Fe, due to these shared neighbors that can prevent the transformation of some cells.

The simulated growth, which is cell by cell, should give a non realistic shape of the crystal but we can consider the evolution of its volume, V (number of cells in the crystal). Although actual nanocrystalline systems may exhibit mainly diffusion controlled growth[1], interface controlled growth is simulated for simplicity, as it was explained above. Therefore, the linear growth should be constant and a double logarithmic representation of the volume transformed (number of cells in the crystal) as a function of time (iteration step) may lead to a slope equal to 3. Fig. 6 shows the growth exponent g of expression $V = \alpha\ t\ g$ obtained from the double logarithmic representation ln(V) vs. ln(t) (see inset) as a function of the Fe content. Whereas for Fe rich alloys a g = 3 is obtained, for poor Fe compositions g goes down to zero. Although linear fittings are enhanced when g is close to 3, the error bars are small enough to supply g values in all the explored range. The particular behavior of 49% composition in the inset is due to those cells that cannot be transformed. For a small crystal the fraction of common neighbors leading to these untransformed cells is large, but once the growing regions are further apart this fraction decreases and the growth exponent increases. This must be understood as a qualitative behavior as it depends on the specific parameters chosen in these simulations.

Fig. 7 shows the local Avrami exponents calculated from unlimited growth simulation experiments performed for different Fe containing systems. In this context, unlimited growth means GL is too large to affect the evolution of the system. The corresponding curves obtained without normalizing the transformed fraction are also shown. Whereas the results obtained from normalized data are in agreement with JMAK theory and a constant n = 4 value is obtained along the transformation, results obtained without normalizing the transformed fraction yields a continuous decrease of the local Avrami exponent. For very low Fe content (≤ 37%), once a cell crystallizes due to nucleation, no further growth is possible as its neighboring cells become exhausted in Fe. This is in agreement with the local Avrami exponent obtained, n ~ 1 along the transformation, indicating constant nucleation rate and absence of growth.

Fig. 8 shows the local Avrami exponents obtained for several values of GL as a function of the normalized transformed fraction. As observed for polymorphic transformations a decrease from n = 4 to n ~ 1 is observed when the growth process becomes impinged, independently of the composition. Exceptions are such very low Fe containing systems for which any growth is prevented even at the very beginning of the process and the Avrami exponent is ~ 1 since the beginning of the process.

5. Discussion

It is worth noticing that at every iteration step some crystals may grow although an Avrami exponent value of 1 should correspond to an absent growth process. However, it is clear that, as time increases, a majority of crystals remains blocked (all those nucleated before a number of iteration steps equal to the maximum growth allowed) and a minority of crystals (as the nucleation rate must decrease as the number of untransformed cells decreases) contributes to the increase of crystalline fraction by growth. The simulation program identifies the number of new nuclei formed as a function of the iteration steps and thus the contributions to crystalline fraction from nucleation and growth can be independently analyzed.

Concerning polymorphic transformations, Fig. 9 shows the number of cells transformed by growth at each iteration step for a 2D 500 × 500 system (with a single nucleation process allowed between each growth process) and different values of GL. For small GL, a plateau is observed with a constant value equal to the sum of the contributions of all growing crystals (for polymorphic transformations every cell is suitable to transform as it does not need any Fe supply from outside). The constant value is an indication of negligible geometrical impingement. In fact, at larger values of crystalline fractions, geometrical impingement is evidenced by some sporadic falls of this value followed by a generalized decrease.

Similar to Fig. 9 and Fig. 10 shows the number of cells transformed by the growth process at each iteration step for non-polymorphic transformations. A higher noise in the data corresponding to non-pure Fe than for pure Fe systems (polymorphic transformations) is due to the fact that the probability for nucleation per iteration step is 1 only for pure Fe systems. In agreement with the results simulated for a single crystal without geometrical impingement, the number of transformed cells by growth is always smaller for the system with 50% than for the 75% Fe containing system.

Generally, deviations from JMAK values to lower ones could be assigned to an underestimation of the impingement effect and analyzed in the frame of a modified kinetic equation [27] :

$$X = 1-\{1 + (\lambda-1)[K(T)(t-t_0)]^n\}^{-\left(\frac{1}{\lambda-1}\right)}$$

where λ is the impingement factor (e.g. λ = 1 for JMAK theory). Using different values of λ, linear fitting were performed on $ln\left[\frac{(1-X)^{-(\lambda-1)}-1}{(\lambda-1)}\right]$ vs. ln(t) plots for (X < 0.8). The best linear fitting for the data shown in Fig. 8 yields the Avrami exponent values shown in Table 1 (the errors in λ indicate the difference between two consecutive values used, for which no significant difference was found). Along with these data, the corresponding impingement factor and the regression coefficient are also shown as well as the impingement factor and the regression coefficient for n = 4. As expected, the impingement factor decreases as the growth limit GL increases. An Avrami exponent close to 4 can be recovered but not for those systems where GL is very low, being n ~ 1.

6. Conclusions

Cellular automata simulations have been performed in two and three dimensional systems to simulate the crystallization process under a limited growth approximation. This approximation resembles several characteristics exhibited by nanocrystalline microstructures and nanocrystallization kinetics and extends the ideas of instantaneous growth approximation to those systems for which a certain growth cannot be neglected. Main conclusions are outlined:

•Avrami exponent can be explained in terms of nucleation and growth processes. At the initial stage of the transformation, Avrami exponent corresponds to a constant nucleation and interface controlled growth processes but it falls down to 1 (absence of growth) at a certain crystalline fraction that decreases as the growth limit decreases.

•JMAK theory is suitable for analysis of non-polymorphic transformations after convenient normalization of the transformed fraction.

•Analysis of the growth process of a single crystal as a function of Fe concentration in the amorphous matrix yields a continuous change of the growth exponent from zero, for very poor Fe compositions, to 3 for rich Fe compositions.

A self-limited growth process is predicted for very poor Fe containing alloys.

Acknowledgements

This work was supported by the Ministry of Science and Innovation (MICINN) and EU FEDER (project. No. MAT2010-20537) and the PAI of the Regional Government of Andalucía (project No. FQM-6462).

References

[1] M.T. Clavaguera-Mora, N. Clavaguera, D. Crespo, T. Pradell

Prog. Mater. Sci., 47 (2002), pp. 559–619

[2] J.H. Perepezko

Prog. Mater. Sci., 49 (2004), pp. 263–284

[3] A. Inoue

Prog. Mater. Sci., 43 (1998), pp. 365–520

[4] D. Zander, U. Köster

Mat. Sci. Eng. A, 375–377 (2004), pp. 53–59

[5] M.E. McHenry, M.A. Willard, D.E. Laughlin

Prog. Mater. Sci., 44 (1999), pp. 291–433

[6] J.S. Blázquez, M. Millán, C.F. Conde, A. Conde

Phil. Mag., 87 (2007), pp. 4151–4167

[7] S.F. Muller

Nanostruc. Mater., 6 (1995), pp. 787–790

[8] Y.G. Zheng, C. Lu, Y.W. Mai, Y.X. Gu, H.W. Zhang, Z. Chen

Appl. Phys. Lett., 88 (2006), pp. 1–3 144103

[9] V. Yamakov, D. Wolf, S.R. Phillpot, H. Gleiter

Acta Mater., 50 (2002), pp. 5005–5020

[10] H.W. Hesselbarth, I.R. Göbel

Acta Metall. Mater., 39 (1991), pp. 2135–2143

[11] H.L. Ding, Y.Z. He, L.F. Liu, W.J. Ding, J. Cryst

Growth, 293 (2006), pp. 489–497

[12] P. Mukhopadhyay, M. Loeck, G. Gottstein

Acta Mater., 55 (2007), pp. 551–564

[13] J.S. Blázquez, V. Franco, C.F. Conde, M. Millán, A. Conde

J. Noncryst. Sol., 354 (2008), pp. 3597–3605

[14] W.A. Johnson, R.F. Mehl

Trans. Am. Inst. Min. Met. Engrs., 135 (1939), pp. 416–458

[15] M. Avrami

J. Chem. Phys., 9 (1941), pp. 177–184

[16] A.N. Kolmogorov

Bull. Acad. Sci. USSR Phys. Ser., 1 (1937), pp. 355–359

[17] K. Nakamura, K. Watanabe, K. Katayama, T. Amano

J. Appl. Polym. Sci., 16 (1972), pp. 1077–1091

[18] K. Nakamura, K. Katayama, T. Amano

J. Appl. Polym. Sci., 17 (1973), pp. 1031–1041

[19] T. Ozawa

Polymer, 12 (1971), pp. 150–158

[20] J.S. Blázquez, C.F. Conde, A. Conde

Acta Mater., 53 (2005), pp. 2305–2311

[21] F. Liu, F. Sommer, C. Bos, E.J. Mittemeijer

Inter. Mater. Rev., 52 (2007), pp. 193–212

[22] J.W. Christian

The Theory of Transformation in Metals and Alloys, Part 1, Pergamon, Oxford (1975), p. 542A

[23] A. Calka, A.P. Radlinski

Mater. Sci. Engng., 97 (1987), pp. 241–246

[24] J.S. Blázquez, M. Millán, C.F. Conde, A. Conde

Phys. Stat. Sol. A, 207 (2010), pp. 1148–1153

[25] I. Sinha, R.K. Mandal, J. Non-cryst

Solids, 355 (2009), pp. 361–367

[26] J.S. Blázquez, J.M. Borrego, C.F. Conde, A. Conde, J.M. Greneche

J. Phys. Condens. Matter, 15 (2003), pp. 3957–3968

[27] M.J. Starink

J. Mater. Sci., 36 (2001), pp. 4433–4441

Figure captions

Figure 1. Microstructure evolution of a 20 × 20 cells region of a 500 × 500 system simulated for unlimited growth (a) and growthlimited to 4 steps (b) as a function of the time (iteration steps), t.

Figure 2. Time evolution of the crystalline fraction (a), Avrami plot (b) and local Avrami exponent as a function of the transformed fraction (c) for unlimited growth and growthlimited to several values for a two dimensional 500 × 500 system.

Figure 3. Time evolution of the crystalline fraction (a), Avrami plot (b) and local Avrami exponent as a function of the transformed fraction (c) for unlimited growth and growthlimited to several values for a three dimensional 50 × 50 × 50 system.

Figure 4. Linear correlation between the saturation value of transformed fraction and the limit value predicted from the balance equation.

Figure 5. Number of cells in a crystal that grows without any impingement as a function of the iteration steps for different content in Fe. Simulation performed in a three dimensional 50 × 50 × 50 cells system.

Figure 6. Growth exponent as a function of the Fe content obtained from the slope of the curves shown in the inset. Simulation performed in a three dimensional 50 × 50 × 50 cells system.

Figure 7. Local Avrami exponent for unlimited growth experiments obtained using the normalized transformed fraction as a function of the transformed fraction (a) and normalized transformed fraction (b) for different Fe content. The local Avrami exponent obtained using directly the transformed fraction is shown for 50 and 75% of Fe (hollow symbols). Simulation performed in a three dimensional 50 × 50 × 50 cells system

Figure 8. Local Avrami exponent for experiments performed using several values of GL in two different compositions and obtained using the normalized transformed fraction. Simulation performed in a three dimensional 50 × 50 × 50 cells system

Figure 9. Number of cells transformed by growth at each iteration step in a two dimensional 500 × 500 cells system. An enhancement is shown below to appreciate simulations with small GL.

Figure 10. Number of cells transformed by growth at each iteration step in a three dimensional 50 × 50 × 50 cells system for two different compositions as a function of the iteration step (a) and the normalized transformed fraction (b).

Table 1

Table 1. Avrami exponent, n, impingement factor, λ, and regression coefficient, r, from linear fittings of $ln\left[\frac{(1-X)^{-(\lambda-1)}-1}{(\lambda-1)}\right]$ vs ln(t)

GL	Best linear fitting			Linear fitting for n = 4	
	n	λ	r	λ	r
8	3.20 ± 0.05	8.2 ± 0.2	0.99392	10.0 ± 0.5	0.99376
13	3.55 ± 0.02	5.5 ± 0.2	0.99837	6.5 ± 0.3	0.99739

Figure 1

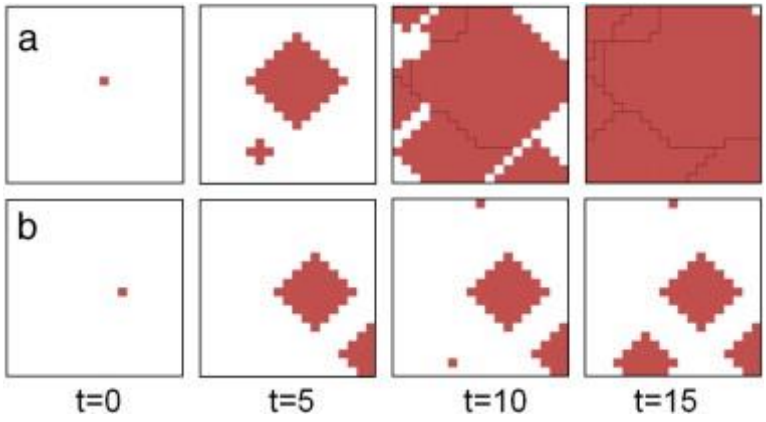

Figure 2

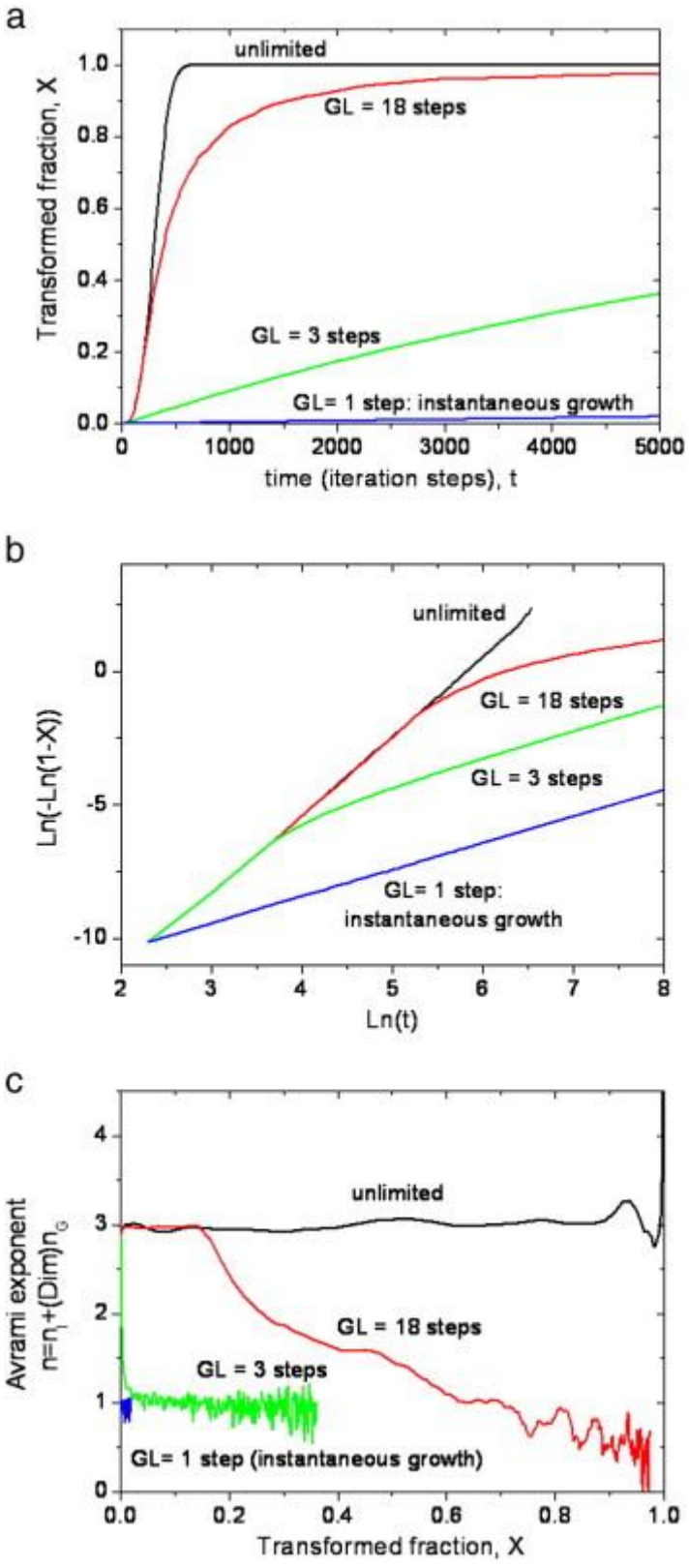
a
unlimited
GL = 18 steps
GL = 3 steps
GL= 1 step: instantaneous growth
Transformed fraction, X
time (iteration steps), t
b
unlimited
GL = 18 steps
GL = 3 steps
GL= 1 step:
instantaneous growth
Ln(-Ln(1-X))
Ln(t)
c
unlimited
GL = 18 steps
GL = 3 steps
GL= 1 step (instantaneous growth)
Avrami exponent
n=n_I+(Dim)n_G
Transformed fraction, X

Figure 3

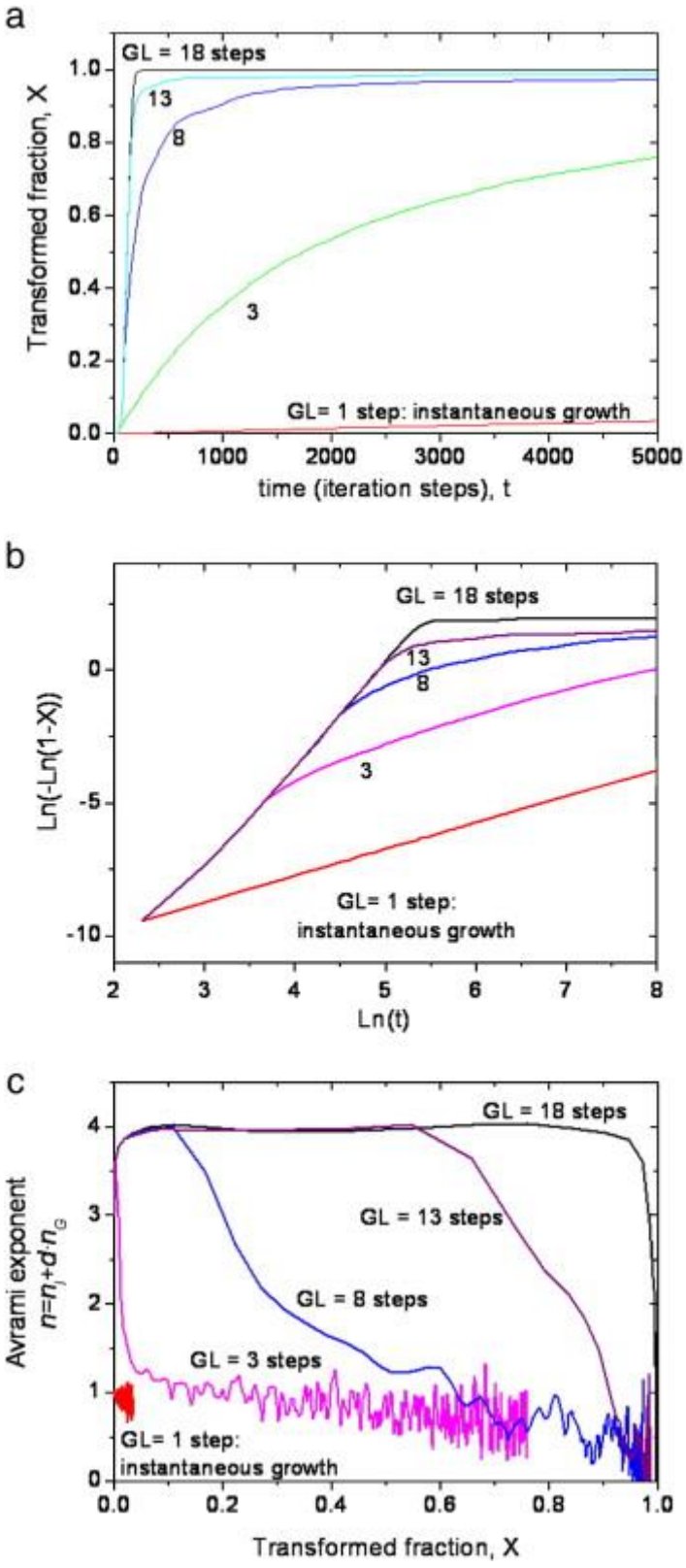
a
GL = 18 steps
13
8
3
GL= 1 step: instantaneous growth
Transformed fraction, X
time (iteration steps), t
b
GL = 18 steps
13
8
3
GL= 1 step:
instantaneous growth
Ln(-Ln(1-X))
Ln(t)
c
GL = 18 steps
GL = 13 steps
GL = 8 steps
GL = 3 steps
GL= 1 step:
instantaneous growth
Avrami exponent
n=n_t+d·n_G
Transformed fraction, X

Figure 4

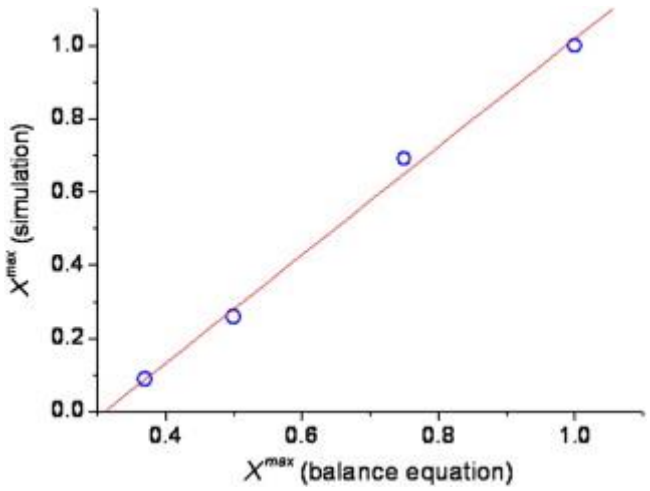
1.0
0.8
0.6
0.4
0.2
0.0
X^{max} (simulation)
0.4
0.6
0.8
1.0
X^{max} (balance equation)

Figure 5

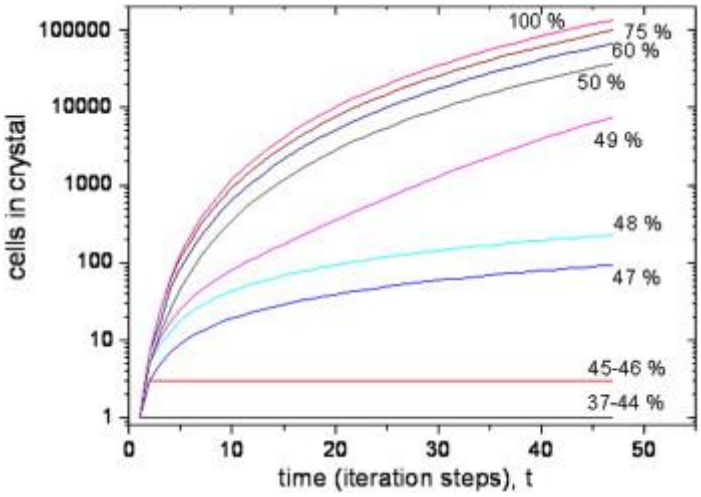
100 %
75 %
60 %
50 %
49 %
48 %
47 %
45-46 %
37-44 %
cells in crystal
time (iteration steps), t
100000
10000
1000
100
10
1
0
10
20
30
40
50

Figure 6

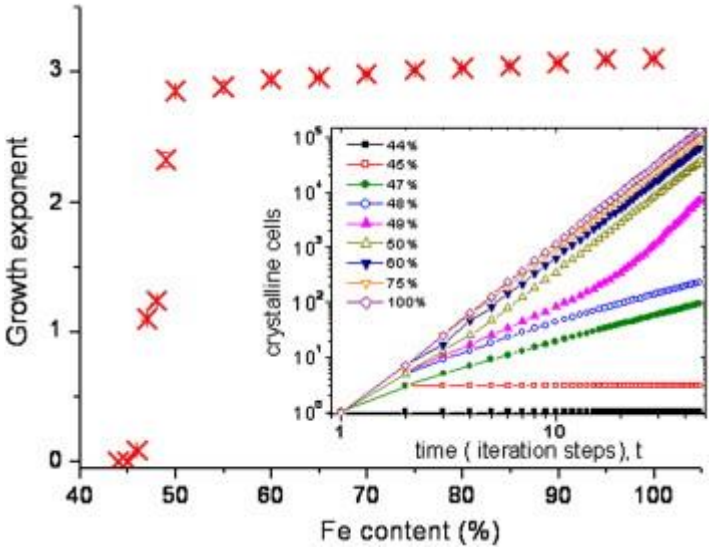
Growth exponent
Fe content (%)
crystalline cells
time (iteration steps), t
44%
45%
47%
48%
49%
50%
60%
75%
100%

Figure 7

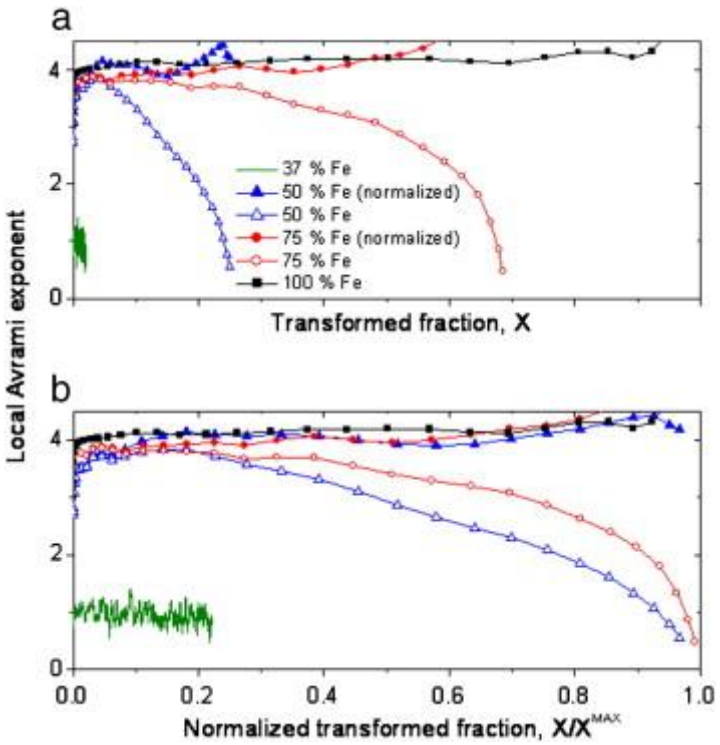
a
b
Local Avrami exponent
Transformed fraction, X
Normalized transformed fraction, X/X^MAX
37 % Fe
50 % Fe (normalized)
50 % Fe
75 % Fe (normalized)
75 % Fe
100 % Fe
0
2
4
0.0
0.2
0.4
0.6
0.8
1.0

Figure 8

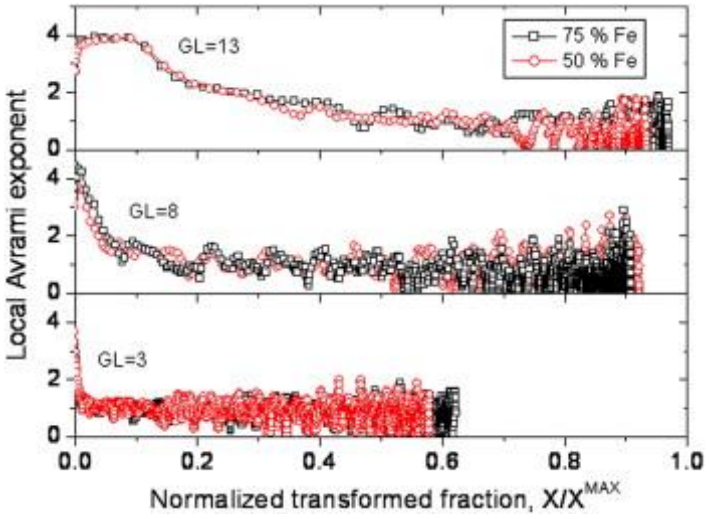
75 % Fe
50 % Fe
GL=13
GL=8
GL=3
Local Avrami exponent
Normalized transformed fraction, X/X^MAX
0.0
0.2
0.4
0.6
0.8
1.0
0
2
4

Figure 9

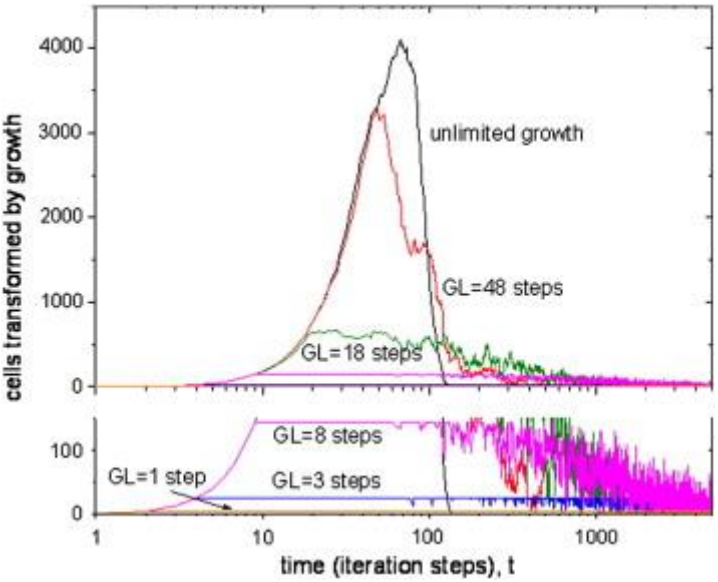
cells transformed by growth
4000
3000
2000
1000
0
unlimited growth
GL=48 steps
GL=18 steps
100
0
GL=8 steps
GL=1 step
GL=3 steps
1
10
100
1000
time (iteration steps), t

Figure 10

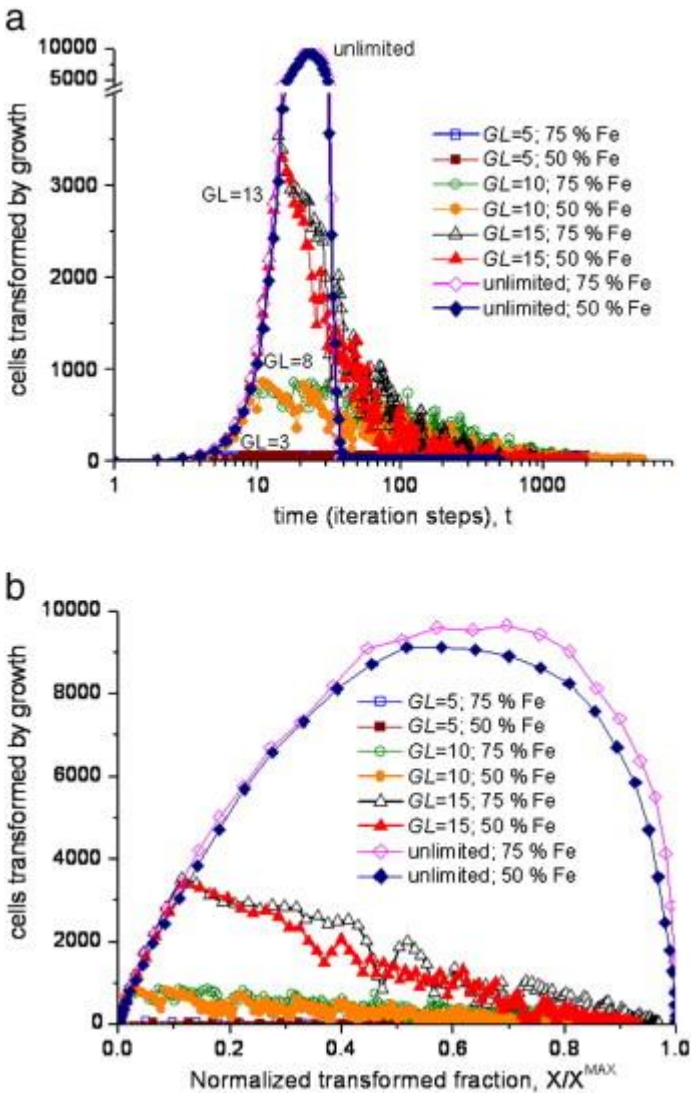
a
10000
5000
3000
2000
1000
0
cells transformed by growth
unlimited
GL=13
GL=8
GL=3
GL=5; 75 % Fe
GL=5; 50 % Fe
GL=10; 75 % Fe
GL=10; 50 % Fe
GL=15; 75 % Fe
GL=15; 50 % Fe
unlimited; 75 % Fe
unlimited; 50 % Fe
1
10
100
1000
time (iteration steps), t
b
10000
8000
6000
4000
2000
0
cells transformed by growth
GL=5; 75 % Fe
GL=5; 50 % Fe
GL=10; 75 % Fe
GL=10; 50 % Fe
GL=15; 75 % Fe
GL=15; 50 % Fe
unlimited; 75 % Fe
unlimited; 50 % Fe
0.0
0.2
0.4
0.6
0.8
1.0
Normalized transformed fraction, X/X^MAX